Appl Phys B (2012) 108:109–115
DOI 10.1007/s00340-012-4979-8

Applied Physics B
Lasers and Optics

Gaussian- versus flat-top-pumping of a mid-IR ZGP RISTRA OPO

M. Eichhorn · G. Stöppler · M. Schellhorn · K.T. Zawilski · P.G. Schunemann

Received: 17 October 2011 / Revised version: 27 January 2012 / Published online: 30 March 2012

Abstract The influence of the pump intensity profile on the performance of a mid-IR ZGP RISTRA OPO at 6.45 μm is studied for a flat-top pump profile and compared to a Gaussian pump distribution at the same pump peak fluence of 0.81 J/cm^2. Due to a coherent beam transformation a flat-top pump beam with a plane wavefront and excellent beam quality of $M^2 \approx 1.25$ is generated. The output of up to 5 mJ pulse idler energy (0.5 W average idler power) is identical in both cases, showing that flat-top pumping allows a reduction of the OPO crystal volume by 55 % while still maintaining a good output beam quality of $M^2 < 2.7$ for the idler and $M^2 < 2.5$ for the signal. The experimental results are compared to the SNLO RISTRA model and the limitations of the model are discussed.

1 Introduction

Mid-infrared optical parametric oscillators (OPOs) are versatile sources for spectroscopy, sensing, countermeasures, and medical applications. Their power scaling is, however, often limited by requirements in beam quality, strongly degrading with pump cross-section scaling due to the large Fresnel numbers then occurring in conventional (linear) OPO resonators. A way to overcome this problem is the Rotated-Image Singly-resonant Twisted-RectAngle (RISTRA) cavity [1–3]. This nonplanar cavity geometry offers a 90° image rotation upon each round-trip causing a lateral phase synchronization or homogenization of the signal wave resonant in that cavity. Therefore, a higher beam quality results while keeping the OPO threshold low compared to an equivalent linear cavity with the same round-trip length. A mid-IR OPO of this type has been studied by Dergachev et al. [4], however, a detailed analysis on beam quality was not performed. A second problem with power scaling is the need to use large aperture crystals to avoid optical damage. For mid-IR materials like $ZnGeP_2$ (ZGP) [5] currently crystals over 10×10 mm^2 are commercially available. As large homogeneous and defect-free crystals are a substantial cost issue, this usually limits the maximum pump beam cross section to avoid cutting off the wings of the Gaussian pump beam. A possible way to overcome this limitation and to increase the useful pump area is a flat-top pump beam. However, the standard methods of flat-top beam generation, e.g., by using phase plates or microlens diffusers, do only provide a homogeneous flat-top intensity profile in a design-specific output plane. This flat-top distribution quickly changes with distance from that plane, and thus would not extend in a collimated way all over the crystal. This is directly linked to the fact that this type of flat-top distribution usually does not possess a well defined or even flat phase front in this image plane. In 2006, Armstrong et al. [2, 3] showed up to 90 % of pump depletion and good beam quality in a nanosecond KTP RISTRA OPO flat-top pumped at 532 nm using pulse-injection-seeding at 803 nm with a flat-top distribution to enhance pump depletion. Therein, a commercial beam transformer (Newport Corporation, GBS-AR16) has been used to generate a flat-top profile from the seed-signal locked to the RISTRA cavity.

M. Eichhorn (✉) · G. Stöppler · M. Schellhorn
French-German Research Institute of Saint-Louis (ISL),
5 rue du Général Cassagnou, BP 70034,
68301 Saint Louis Cedex, France
e-mail: Marc.Eichhorn@isl.eu

K.T. Zawilski · P.G. Schunemann
BAE Systems, P.O. Box 868, MER15-1813, Nashua,
NH 03061-0868, USA

Over many years, OPOs were mainly pumped by narrow or even single-longitudinal-mode lasers, and for this case a numerical RISTRA model for SNLO has been developed which is available free of charge [6]. It has been suggested in [4] that the SNLO model may give at least some design guidance for RISTRA performance in case of a multilongitudinal mode pump operation. For medical applications, however, a laser or OPO system needs to provide a certain output pulse energy or average power, to be robust, not too expensive, i.e., not too complex in its setup, and to be operated in a regime that allows long operation times before failure. Thus, a multilongitudinal-mode pump laser, which is much easier to build, and a nonseeded OPO operation is targeted. Therefore, ultra-high efficiency and pump depletion are less important in this case. Also, a low threshold and therefore a low optical damage probability is of advantage.

In this paper, we present a comparison of flat-top versus Gaussian beam pumping of a mid-IR ZGP RISTRA OPO wherein the flat-top beam is created by a coherent beam transformer using aspheric lenses, generating a flat phase front of the pump which allows keeping the pump intensity distribution preserved over a substantial propagation distance. Signal and idler waves are unseeded and result only from the properties of the RISTRA cavity. In addition, a thorough comparison between the SNLO RISTRA model and experimental results are performed for the corresponding Gaussian pump profile, showing the limitations of single-longitudinal-line modeling on predicted OPO performance.

2 Design of the coherent beam transformer

Although probably somehow similar to the commercial version from Newport also using aspheric lenses, our design presented here has been specifically addressed to the 2 µm wavelength region, where the commercially available systems cannot be used. It also has to be taken into account that important design considerations, e.g., the edge slope of the flat-top distribution, will lead to a specific design differing from the commercial version. Therefore, the design of the beamshaper used will be discussed in detail in the following. The coherent beam transformer is based on two plano-aspheric lenses in a telescopic arrangement. The first lens therein creates a super-Gaussian intensity distribution at the position of the second lens by redistributing the beam intensity of the Gaussian input. The second lens then corrects the phase distribution of the Super-Gaussian profile so that this profile is emitted as a collimated beam. Therefore, this kind of coherent beam transformer allows the generation of a flat-top beam with a very long axial extension of the flat-top zone before diffraction deteriorates this profile.

To determine the necessary aspheric lenses, the input and output beam parameters have to be defined. In this case,

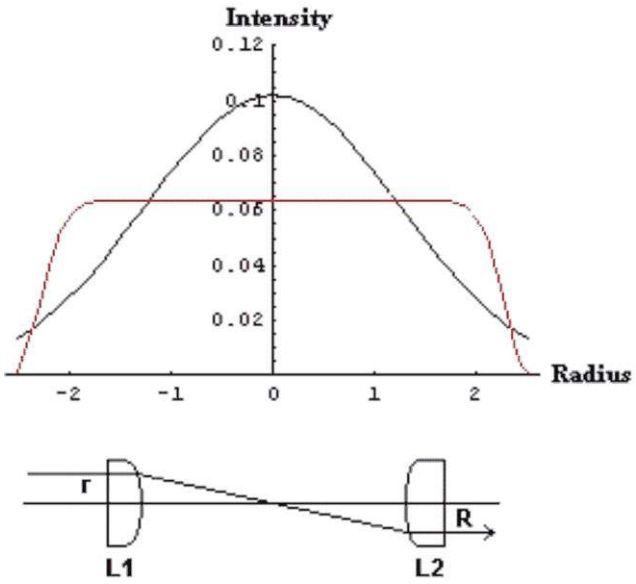

Fig. 1 Comparison of a Gaussian beam ($p = 2$) with its equivalent Super-Gaussian profile ($p = 16$) after the transformation

it is advantageous to choose both beam diameters to be of the same order of magnitude, as shown in Fig. 1. The aspheric surfaces then contribute nearly equally to the refractive power over the lens radius and, therefore, only small gradients occur. The super-Gaussian profile is given by

$$g(r) = g_0 e^{-2(\frac{r}{R_0})^p} \tag{1}$$

with the normalization constant

$$g_0 = \frac{p 2^{\frac{2}{p}}}{2\pi {R_0}^2 \Gamma(\frac{2}{p})}. \tag{2}$$

As the initial calculation of the coherent beam transformal has been performed to pump a 5 mm diameter crystal; a super-Gaussian of $R_0 = 2.4$ mm and $p = 16$ was chosen. Therein the value of p determines the slope of the wings in the distribution. This parameter should therefore be chosen to be large enough to allow for a maximum area of the homogeneously illuminated flat-top region. However, a too large p will lead to stronger diffraction effects, and thus limit the useful axial range of collimation of the flat-top profile. For the Gaussian input,

$$f(r) = f_0 e^{-2(\frac{r}{w_0})^2} \tag{3}$$

with the normalization

$$f_0 = \frac{2}{\pi {w_0}^2} \tag{4}$$

a radius of $w_0 = 2.5$ mm was chosen.

Now the optical path between the two lenses can be calculated according to the theory in [7, 8]. The intensity transformation generated by the first lens is defined by the input and output beam parameters. Therefore, a photon exiting the

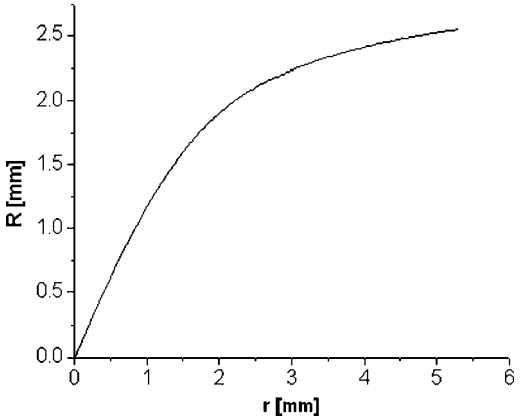

Fig. 2 Imaging function $R(r)$ necessary for the determination of the sag curves. In the Keplerian case, the sign has to be reversed

first lens at radius r has to hit the second lens at radius R, and due to the conservation of energy within the beam, we obtain the relation

$$\int_0^{R(r)} g(x)x\,dx = \int_0^{r} f(x)x\,dx, \tag{5}$$

defining the imaging function $R(r)$ that is depicted in Fig. 2. Using the refractive index $n = 1.44298$ of the lens material (Infrasil) and the chosen distance between both lenses of $D = 150$ mm, one obtains the necessary lens surface [9]:

$$z_1(r) = \int_0^{r} \frac{1}{\sqrt{n^2 - 1 + (\frac{(n-1)D}{R(x)-x})^2}}\,dx \tag{6}$$

$$z_2(r) = \int_0^{r} \frac{1}{\sqrt{n^2 - 1 + (\frac{(n-1)D}{R^{-1}(x)-x})^2}}\,dx. \tag{7}$$

Therein, $z_1(r)$ is the sag of the input lens, $z_2(r)$ the sag of the output lens and $R^{-1}(x)$ the inverse function of $R(x)$. This calculation results in the sag curves given in Fig. 3.

Due to the rotational symmetry r and $R(r)$ in Eq. 5 can have the same or opposite signs. The first case leads to a Galilean telescope, the second one to a Keplerian telescope with an intermediate focus. Concerning lens fabrication the Keplerian type results in convex-only surfaces that are much easier to manufacture. The Galilean lenses possess much more complex surface features and, therefore, might only be considered when the overall length or the focal point in the system is a concern.

3 Experimental setup

The experimental setup depicted in Fig. 4 consists of a high-pulse-energy Ho^{3+}:LLF laser system [10] including an additional amplifier stage, thus delivering up to 68 mJ of pulse energy at 100 Hz repetition rate and a pulse duration of 38 ns as the pump source. The Gaussian output beam ($M_x^2 = 1.01$

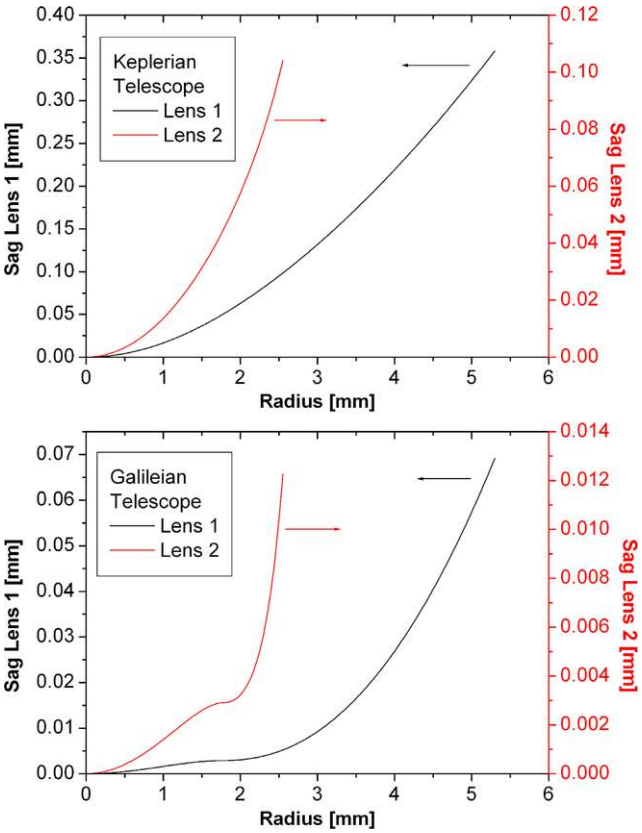

Fig. 3 Sag curves of the aspheric lenses in the Keplerian (*top*) and Galileian case (*bottom*)

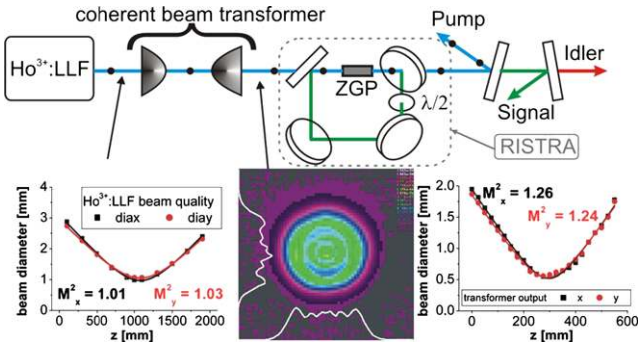

Fig. 4 Schematic outline of the experimental setup. The *insets* show the beam quality before and after the beam transformer and the intensity profile of the flat-top beam

and $M_y^2 = 1.03$, where x denotes the critical axis and the polarization direction of the pump in the ZGP crystal) is either directly used as the pump beam or enters, as shown in Fig. 4, a coherent Gaussian-to-flat-top beam transformer consisting of the two aspheric lenses calculated in Sect. 2 for the Keplerian case. Both lenses are antireflection coated for the 2.05 µm pump wavelength resulting in a beam transformer transmission of 96 %. The aspheric surfaces have been optimized for transforming a 5 mm diameter ($1/e^2$) Gaussian

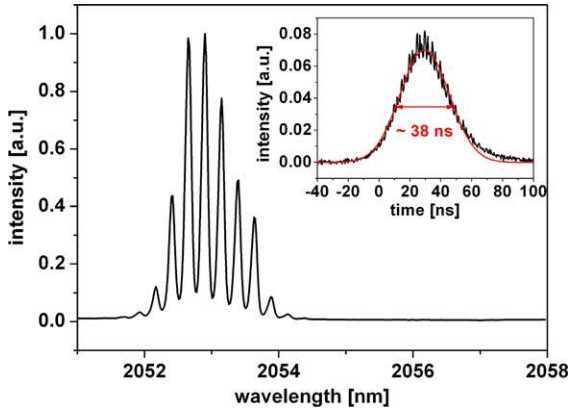

Fig. 5 Measured output spectrum of the Ho^{3+}:LLF pump beam showing its multiline emission spectrum. The *inset* shows the temporal pulse shape

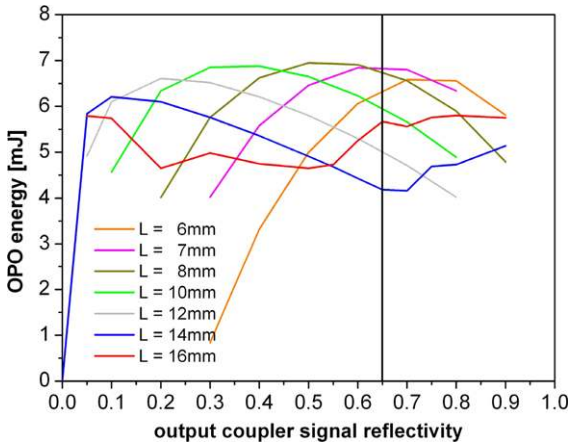

Fig. 6 Numerical simulation of the idler energy at 44 mJ incident pump energy (Gaussian beam) and the $L = 16$ mm long ZGP crystal at different signal outcoupling reflectivities

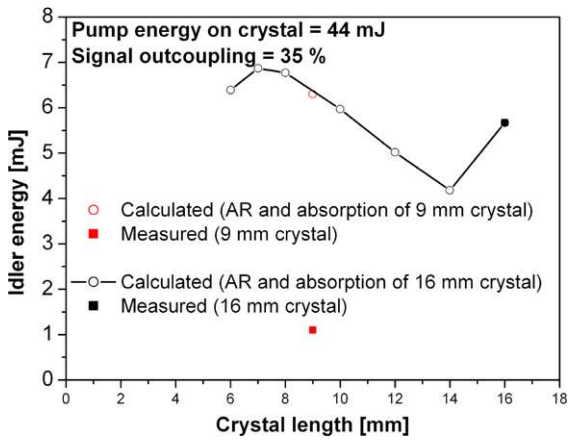

Fig. 7 Numerical simulation of the idler energy at 44 mJ incident pump energy (Gaussian beam) at 65 % signal OC reflectivity for different crystal lengths

input beam into a 5 mm diameter flat-top beam with plane output wave front.

Due to a slight mismatch between the output beam diameter of the Ho^{3+}:LLF system of 3.85×3.65 mm^2 $(1/e^2)$ and the design specifications of the beam transformer the flat-top output beam shows an annular modulation in its flat intensity profile which can be seen in Fig. 4 and measures 3.30×3.15 mm^2. Measuring the beam diameter in both directions using the 90/10 knife-edge method through the focus of the output beam produced by a lens results in a beam-propagation factor of $M_x^2 = 1.26$ and $M_y^2 = 1.24$. This shows the extremely good beam quality achieved by the coherent beam transformation and the close-to-plane output wave front.

The emission spectrum of the Ho^{3+}:LLF laser depicted in Fig. 5 shows a clear operation on several spectral lines. The OPO pump laser therefore has to be considered to operate on a very large number of longitudinal modes. The beating of these modes can be clearly seen on the temporal pulse shape taken by a fast detector and also shown in Fig. 5.

The RISTRA cavity is placed behind the beam transformer at a distance such that the beam profile shown in Fig. 4 with a diameter of 3.30×3.15 mm^2 is the incident pump profile on the ZGP crystal. The cavity is singly-resonant on the 3.01 µm signal wave with an outcoupling of 35 % and transmits >98 % of the idler wave at 6.45 µm. The ZGP single crystal of size $7 \times 7 \times 16$ mm^3 (Eksma, Lithuania) is AR coated at pump, signal, and idler and mounted into an uncooled copper heatsink using indium foil. The residual pump absorption of this crystal has been determined to $\alpha = 0.053$ cm^{-1}.

4 Results and discussion

A numerical simulation of the RISTRA has been performed using the SNLO model taking into account all parameters of the ZGP crystal and the cavity. Assuming 44 mJ of incident pump energy the OPO idler output energy has been calculated as a function of output coupling signal reflectivity for different crystal lengths (6–16 mm). The results are shown in Fig. 6. The model predicts an optimum output of ~7 mJ for signal reflectivities of 50–60 %. The curves for the >12 mm long crystals deviate from the general parabolic shape of the shorter crystals. This is due to numerical instabilities occurring because the grid size used in the calculation (32 in z and 64 in xy) becomes too coarse for the high gain associated with the long crystals. The reflectivity of the dielectric coating came out to be 65 %, which should not be too high and should result in a low threshold for the OPO and, therefore, a reduced risk of optical damage.

A first experiment with a $L = 9$ mm long ZGP crystal ($\alpha = 0.073$ cm^{-1}) was conducted in order to verify the simulation prediction. As can be seen in Fig. 7, the simulation, however, excessively overestimates the experimental mea-

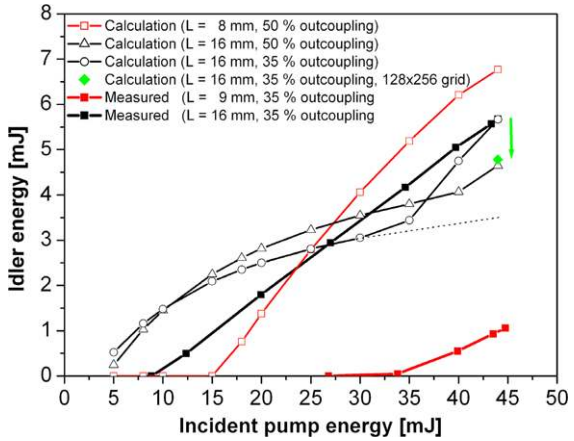

Fig. 8 Numerical simulation of the idler energy at 44 mJ incident pump energy (Gaussian beam) for different crystal lengths, signal outcouplings, and simulation grid sizes versus pump energy

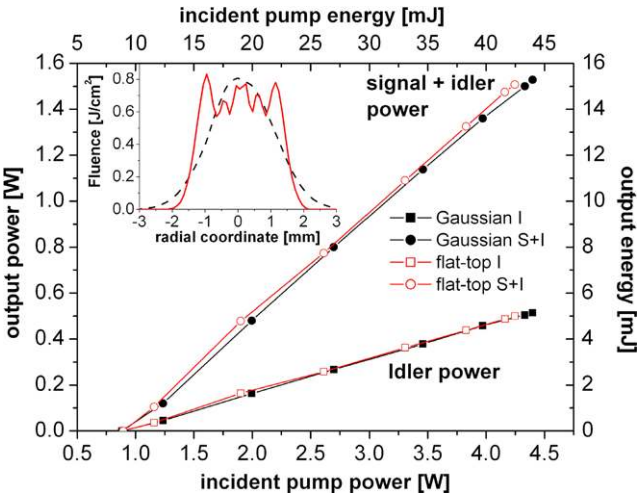

Fig. 9 Measured output average power or energy of the OPO (total power or energy and idler) versus incident pump average power or energy at 100 Hz repetition rate. The *inset* shows the fluence profiles for both pump beams

surements (6.3 mJ vs. 1.1 mJ). As the simulation's temporal and spatial output profiles showed no evidence of numerical instabilities for this crystal, it was assumed that due to the low spectral brightness and low coherence of the pump laser compared to the single-longitudinal-mode case covered by SNLO, the prediction was rather incorrect. Therefore, a second experiment was conducted employing the above-mentioned 16 mm long ZGP crystal. The measured output pulse energy of 5.67 mJ at 44 mJ of pump energy perfectly matches the simulated result, however, on a curve that does show strong numerical instabilities.

A detailed analysis of the output energy curves is shown in Fig. 8. It predicts that doubling the crystal length reduces the threshold, but also the slope and conversion efficiency due to strong back conversion. It also shows that the perfect match occurs by accident, as the numerical instabilities start at around 30–35 mJ of pump energy for 35 % outcoupling. Increasing the grid to 128 in z and 256 in xy reduces the simulation output to 4.78 mJ, thus coming closer to the expected behavior (dotted line). It is, however, impractical to increase the grid-size enough to be able to simulate the correct output energy of the 16 mm long ZGP crystal in this arrangement at 44 mJ pump energy due to available computer resources. It can also be seen that the experimental values show a completely different behavior than the calculation: The output power corresponds to a straight line rather than a curve with a decreasing slope like in the simulations, which is a result of back conversion due to sum-frequency mixing between signal and idler generating unuseful pump radiation that is 180° out of phase to the original pump. The straight line observed up to our maximum available pump energy, being 5.5 times above threshold, shows that no back conversion occurs. This main difference, despite the large differences between measurement and simulation seen for the 9 mm crystal, leads us to the conclusion that in multiple-longitudinal-mode operation a RISTRA OPO cannot be simulated like in single-longitudinal-mode operation. The reason therefore may be twofold. First, it could be seen during the experiments that the output spectra in signal and idler become increasingly broad with increasing pump power. Second, due to the much lower spectral brightness of the pump source, this results in conditions that significantly reduce the effect of back conversion. As the OPO process is a coherent process, the conversion between the involved fields strongly depend on the number of photons per mode, i.e., the spectral coherence of the involved fields. The broadening of the spectra reduces this coherence and, therefore, partially compensates for the increasing field strengths with increasing pump power. Back conversion thus is no problem in the presented arrangement and explains the long crystal lengths employed in our investigations.

In the scope of this work, the OPO performance with the flat-top pump beam is to be compared to the one using a Gaussian beam of identical peak fluence as this is the limiting parameter in terms of optical damage. To be still safe for the crystal used, a pump peak fluence of 0.808 J/cm^2 is chosen in the Gaussian case while for the flat-top beam a peak fluence of 0.82 J/cm^2 is measured. This results in the two beam profiles shown in the inset of Fig. 9. There it can be seen that for negligible pump aperture losses a crystal of 4×4 mm^2 is sufficient in the flat-top case while 6×6 mm^2 would be necessary in order to not cut into the Gaussian beam. The experimental results for both pump conditions are, however, identical with respect to average powers and pulse energies as shown in Fig. 9. At the repetition rate of 100 Hz up to 0.5 W of average power (5 mJ of pulse energy) is obtained in the idler wave. The OPO threshold of 8.9 mJ is also identical in both cases. This shows that the conversion to a flat-top pump profile has no negative effect

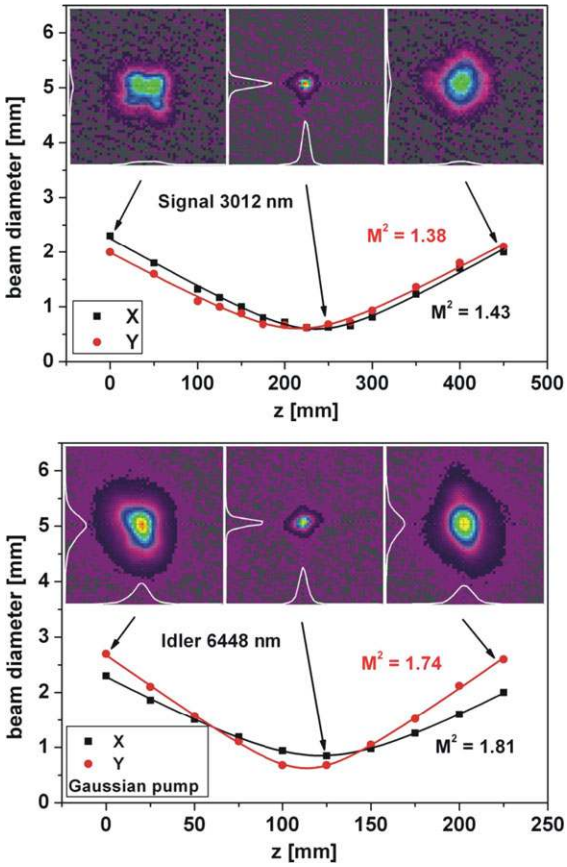

Fig. 10 Beam propagation factor measurement for signal and idler in the case of the Gaussian pump beam at 5.15 mJ per idler pulse

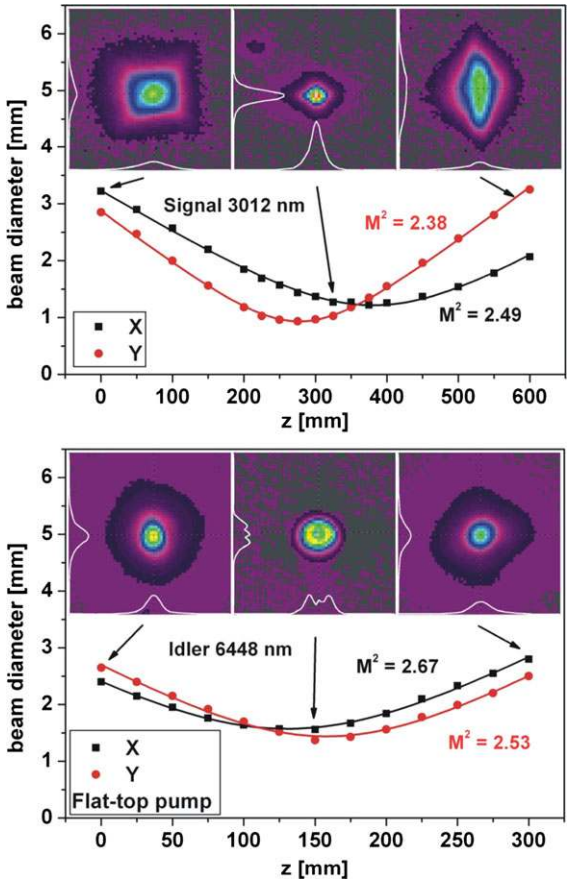

Fig. 11 Beam propagation factor measurement for signal and idler in the case of the flat-top pump beam at 5.0 mJ per idler pulse

on OPO power performance and allows in principle smaller crystal cross sections to be used.

However, in some applications also the beam quality is important. In a first experiment, the RISTRA is pumped by the Gaussian beam and the beam propagation factor is determined by measuring the beam diameter obtained from a 90/10 knife-edge analysis through the focus of a lens, depicted in Fig. 10. This results in $M_x^2 = 1.43$ and $M_y^2 = 1.38$ for the signal beam and $M_x^2 = 1.81$ and $M_y^2 = 1.74$ for the idler wave at maximum energy. This good beam quality is the result of the lateral phase synchronization of the RISTRA cavity due to the 90° image rotation per round trip. This image rotation also is responsible for the square-like symmetry of the signal beam profile seen in the left inset of Fig. 10 which shows the beam close to the RISTRA exit. In the far field, i.e., in the focus of the lens and after propagation trough the focus the signal beam becomes more Gaussian due to diffraction self-cleaning. The idler, which itself is not resonant in the cavity and, therefore, does not see any constraints or influence from the image rotation, shows a profile that is much closer to a Gaussian beam already at the exit of the RISTRA. It can also be noted that both waves generated by the OPO do not show a strong astigmatism. A calculation taking into account the thermal properties of ZGP ($\frac{\partial n_e}{\partial T}(3.01\ \mu\text{m}) = 1.705 \times 10^{-4}\ \text{K}^{-1}$, $n_e(3.01\ \mu\text{m}) = 3.167$ and $\lambda_{th} = 35.5\ \text{W m}^{-1}\,\text{K}^{-1}$ from [11]) results in a temperature rise of $\Delta T = 0.14$ K and a thermal lens of $f = 6.94$ m, and thus a signal cavity mode diameter of 2.2 mm on the crystal. For the idler, this yields a diameter of 3.64 mm on the crystal. The aberration induced by this thermal lens and the smaller signal mode compared to the pump cross section can thus be made responsible for the beam quality values found.

For flat-top pumping the beam-propagation factors depicted in Fig. 11 are determined to $M_x^2 = 2.49$ and $M_y^2 = 2.38$ for the signal beam and $M_x^2 = 2.67$ and $M_y^2 = 2.53$ for the idler wave using the same method as before. Again, the signal beam close to the OPO exit shows the square-like symmetry from the image-rotation effect which disappears during propagation. The signal also exhibits a strong astigmatism, for which the origin is currently unclear. In principle, this could be a thermal lens effect within the ZGP crystal. However, the flat-top pump profile should result in a much more homogeneous heat load compared to the Gaussian pump and, therefore, the thermal lens induced by flat-top pumping should show less aberrations than in the previ-

ous case. The thermo-optic calculation for the flat-top case results in a temperature rise of $\Delta T = 0.13$ K and a thermal lens of $f = 9.6$ m and thus a signal cavity mode diameter of 3.12 mm on the crystal. For the idler, this yields a diameter of 4.74 mm on the crystal. The much more homogeneous pump distribution in the flat-top case results in a less strong thermal lens compared to the Gaussian pump, although the pump spot is smaller. However, the beam quality degradation by the beam transformer, i.e., the not completely flat phase front, results in a much larger M^2 than in the Gaussian case. An interesting effect is seen in the focus of the idler beam in Fig. 11. The pump profile is found back in the idler profile which results from the singly-resonant nature of this OPO. While the signal beam is locked onto the resonant cavity the OPO can transfer excess entropy (e.g., beam quality, phase distribution, etc.) onto the idler which is only restricted by energy and momentum conservation, but has no additional conditions imposed by, e.g., a cavity.

5 Conclusion

In conclusion, the performance of a mid-IR RISTRA OPO has been studied under comparable pump peak fluences using Gaussian and flat-top pump beams. It has been shown that in terms of pulse energy and output power both configurations are identical. Therefore, a smaller crystal cross section can be employed by using a pump beam transformation. Concerning beam quality, a slight degradation is found for the flat-top pump compared to the Gaussian pump which is mainly a result of the degradation in pump beam quality of the flat-top beam. Thermal lensing is, however, weaker in the flat-top case. For a singly-resonant RISTRA OPO the flat-top pump profile is imprinted onto the idler wave while the resonant signal shows a more Gaussian-like profile due to the influence of the cavity. Significant astigmatism of the signal has been found for flat-top pumping, which is subject to further investigation. Although the crystal lengths used seemed at first sight to be quite large, if not too large and, therefore, should lead to excessive back conversion, it was found that modelling of RISTRA OPOs based on single-longitudinal-mode calculations can result in wrong guidelines for design. This mainly results from the fact that due to the coherent OPO interaction the spectral brightness of all involved fields play an important role. While the extremely high spectral brightness in single-longitudinal-mode operation results in strong back conversion, broad-band multi-longitudinal-mode operation can compensate for this effect, and thus can allow high output pulse energies without too high back conversion.

Acknowledgements The research leading to these results has received funding from the European Community's Seventh Framework Programme FP7/2007-2011 under grant agreement n° 224042.

References

1. A.V. Smith, D.J. Armstrong, J. Opt. Soc. Am. B, Opt. Phys. **19**, 1801 (2002)
2. A.V. Smith, D.J. Armstrong, Opt. Lett. **31**, 380 (2006)
3. D.J. Armstrong, A.V. Smith, IEEE J. Sel. Top. Quantum Electron. **13**, 721 (2007)
4. A. Dergachev, D. Armstrong, A. Smith, T. Drake, M. Dubois, Opt. Express **15**, 14404 (2007)
5. K.T. Zawilski, P.G. Schunemann, S.D. Setzler, T.M. Pollak, J. Cryst. Growth **310**, 1891 (2008)
6. SNLO program, http://as-photonics.com/RISTRA-Modeling.html, AS Photonics, LLC
7. J.A. Hoffnagle, C.M. Jefferson, Appl. Opt. **39**, 5488 (2000)
8. J.A. Hoffnagle, C.M. Jefferson, Opt. Eng. **42**, 3090 (2003)
9. J.L. Kreuzer, Coherent light optical system yielding an output beam of desired intensity distribution at a desired equiphase surface. U.S. patent 3,476,463 (1969)
10. M. Schellhorn, Opt. Lett. **35**, 2609 (2010)
11. D.N. Nikogosian, *Nonlinear Optical Crystals: A Complete Survey* (Springer, New York, 2005). ISBN: 0-387-22022-4